Kinesin-1 mediates translocation of the meiotic spindle to the oocyte cortex through KCA-1, a novel cargo adapter

Hsin-ya Yang,[1] Paul E. Mains,[2] and Francis J. McNally[1]

[1]Section of Molecular and Cellular Biology, University of California, Davis, Davis, CA 95616
[2]Department of Biochemistry and Molecular Biology, Genes and Development Research Group, University of Calgary, Calgary, Alberta T2N 4N1 Canada

In animals, female meiotic spindles are attached to the egg cortex in a perpendicular orientation at anaphase to allow the selective disposal of three haploid chromosome sets into polar bodies. We have identified a complex of interacting *Caenorhabditis elegans* proteins that are involved in the earliest step in asymmetric positioning of anastral meiotic spindles, translocation to the cortex. This complex is composed of the kinesin-1 heavy chain orthologue, UNC-116, the kinesin light chain orthologues, KLC-1 and -2, and a novel cargo adaptor, KCA-1. Depletion of any of these subunits by RNA interference resulted in meiosis I metaphase spindles that remained stationary at a position several micrometers from the cell cortex during the time when wild-type spindles translocated to the cortex. After this prolonged stationary period, *unc-116(RNAi)* spindles moved to the cortex through a partially redundant mechanism that is dependent on the anaphase-promoting complex. This study thus reveals two sequential mechanisms for translocating anastral spindles to the oocyte cortex.

Introduction

Meiosis is essential for sexual reproduction in all eukaryotes. During meiosis, a replicated diploid genome is reduced to four haploid genomes through two consecutive rounds of chromosome segregation. In females of both plants and animals, three haploid genomes are discarded and only one haploid genome is inherited by a female gamete. In animals, this asymmetric inheritance is mediated by spindles that are attached by one pole to the oocyte cortex during anaphase. In most animals, this perpendicular attachment to the cortex allows segregation of three haploid genomes into tiny cells called polar bodies and segregation of one haploid genome into a large egg, thus reserving almost all of the oocyte's cytoplasm for embryo development (Selman, 1966; Maro and Verlhac, 2002).

Detailed studies of meiotic spindle movements in mouse (Maro et al., 1984, 1986; Verlhac et al., 2000) and *Caenorhabditis elegans* (Yang et al., 2003) have revealed a conserved series of movements that include translocation of the spindle to the cortex and rotation of the spindle from a parallel to a perpendicular orientation to allow chromosome segregation into a polar body. Movement and orientation of mitotic spindles in animals and fungi is thought to occur through astral microtubules that emanate from centriole-containing centrosomes or spindle pole bodies (Gonczy, 2002; Sheeman et al., 2003). However, the female meiotic spindles of humans (Sathananthan, 1997), cows (Navara et al., 1994), mice (Gueth-Hallonet et al., 1993), *Drosophila melanogaster* (Theurkauf and Hawley, 1992), and *C. elegans* (Albertson and Thomson, 1993) do not have centrioles or their associated astral microtubule arrays.

Mice and *C. elegans* have evolved different mechanisms for translocating their meiotic spindles to the oocyte cortex in the absence of astral microtubule arrays. Translocation of the mouse meiosis I spindle to the cortex is dependent on F-actin and c-mos but does not require microtubules (Verlhac et al., 2000). In contrast, we have previously shown that translocation of the *C. elegans* meiosis I spindle is dependent on microtubules and the microtubule-severing enzyme MEI-1 but is not dependent on F-actin (Yang et al., 2003). In both cases, the mechanism that polarizes cytoskeletal filaments toward the cortex and the mechanism of movement are unknown.

The microtubule dependence of *C. elegans* meiotic spindle translocation suggested that one or more microtubule motor proteins would be required either to establish bipolarity of spindle microtubules or to directly transport the spindle on the cytoplasmic microtubule array. To identify this motor (or motors), we initiated an RNA interference (RNAi) screen of the 23

Correspondence to Francis J. McNally: fjmcnally@ucdavis.edu

Abbreviations used in this paper: APC, anaphase-promoting complex; RNAi, RNA interference.

The online version of this article includes supplemental material.

The Journal of Cell Biology, Vol. 169, No. 3, May 9, 2005 447–457
http://www.jcb.org/cgi/doi/10.1083/jcb.200411132

microtubule motor subunits encoded in the *C. elegans* genome. We identified UNC-116, the kinesin-1 heavy chain (Patel et al., 1993), as essential for normal translocation of the meiotic spindle to the cortex. Because meiotic spindle structure appears normal in UNC-116–depleted embryos, this result suggests that the spindle is translocated on the acentrosomal cytoplasmic microtubule array. Such directional transport on an acentrosomal microtubule array is also observed during mRNA localization in *D. melanogaster* oocytes (Cha et al., 2001) and vesicle transport in plant cells (Gunning and Steer, 1996).

Results

In *unc-116(RNAi)* embryos, the meiotic spindle remains stationary during the period when wild-type spindles translocate to the cortex

To determine whether or not microtubule motor proteins are involved in the translocation of the meiotic spindle to the oocyte cortex in *C. elegans*, we analyzed meiotic spindle translocation in worms depleted of different motor subunits by RNAi. There are 21 kinesin motor-domain homologues and two dynein heavy chain subunits encoded in the *C. elegans* genome (Wormbase). We recorded time-lapse sequences of meiotic spindle movements in worms expressing GFP-tubulin and that were treated with double-stranded RNA corresponding to seven different kinesin motor-domain homologues (UNC-116/R05D3.7, KLP-3/T09A5.2, KLP-7/K11D9.1, BMK-1/F23B12.8, KLP-15/M01E11.6, KLP-18/C06G3.2, and KLP-20/Y50D7A.6). Defective meiotic spindle translocation was observed only in *unc-116(RNAi)* worms. UNC-116 is the *C. elegans* orthologue of kinesin-1 heavy chain (Patel et al., 1993; Lawrence et al., 2004). Maturing *C. elegans* oocytes move into a somatic structure called the spermatheca after germinal vesicle breakdown, and then squeeze out of the other side of the spermatheca into the uterus. In the examples shown in Fig. 1 (A and B), the wild-type spindle contacted the cortex 42 s after exit from the spermatheca, whereas the *unc-116(RNAi)* spindle contacted the cortex 8.2 min after exit from the spermatheca. Similar results were obtained from 27/27 time-lapse sequences of wild-type worms and 15/19 time-lapse sequences of *unc-116(RNAi)* worms (Table I).

Careful analysis of the distance of the meiotic spindle from the cortex over time (Fig. 1, C and D) revealed that *unc-116(RNAi)* spindles remain completely stationary for up to 8 min after exit from the spermatheca, whereas wild-type spindles begin movement toward the cortex before the zygote exits from the spermatheca. An example of this prolonged stationary

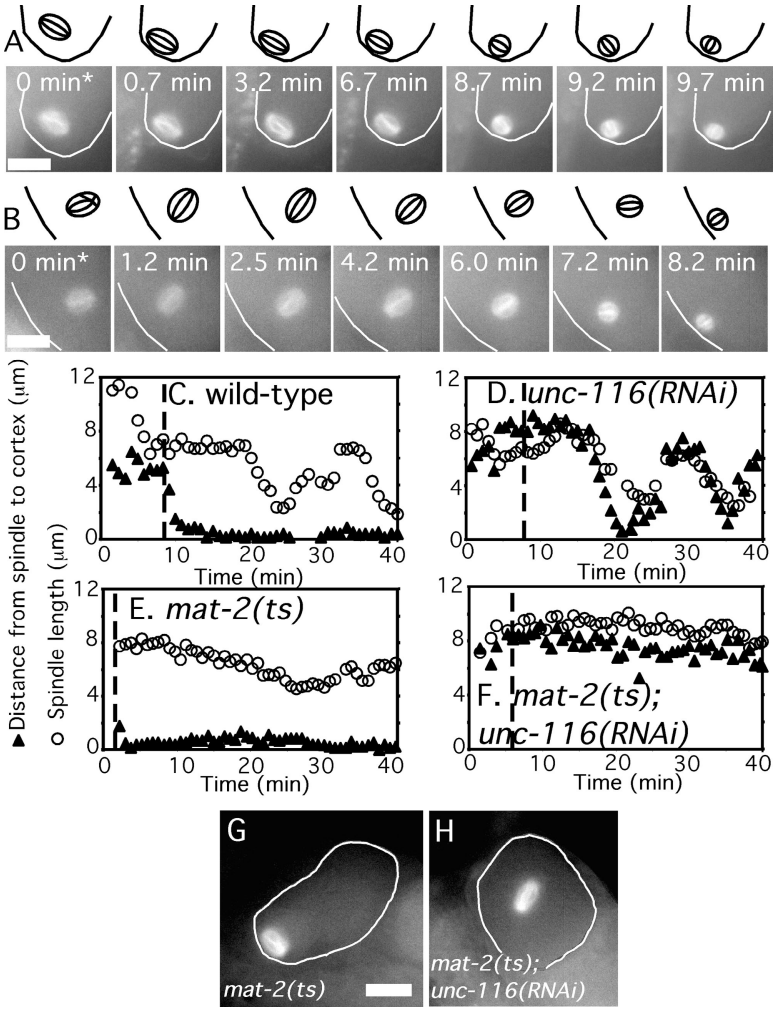

Figure 1. ***unc-116(RNAi)* spindles are stationary during the period of meiosis when wild-type spindles translocate to the cortex.** Images of GFP-tubulin fluorescence within a meiotic embryo are shown from representative time-lapse sequences from a wild-type worm (A) and an *unc-116(RNAi)* worm (B). The cell cortex was highlighted in each image and drawings corresponding to each image are included for clarity. (A) The wild-type meiosis I spindle translocated to the cortex from 0 to 0.7 min and adopted an orientation parallel to the cortex until spindle rotation from 8.7 to 9.7 min. (B) In contrast, the meiosis I spindle in the *unc-116(RNAi)* embryo remained stationary at a position several micrometers from the cortex from 0 to 6.0 min. Spindle shortening initiated just before the start of movement to the cortex (6.0 to 7.2 min) in the *unc-116(RNAi)* embryo, in contrast with the wild-type spindle, which initiated shortening long after cortical contact. Time 0 indicates exit of the zygote from the spermatheca into the uterus. Corresponding Videos 1 and 2 can be found in the online supplemental material available at http://www.jcb.org/cgi/content/full/jcb.200411132/DC1. (C–F) The shortest distance from the edge of the spindle to the cortex (▲) and the pole–pole spindle length (○) was measured in each frame of one representative GFP-tubulin time-lapse sequence from embryos of the indicated genotype. Time 0 is germinal vesicle breakdown. The vertical dotted line indicates the time the embryo exited the spermatheca into the uterus. (C) In wild-type embryos, spindle movement to the cortex initiated before exit from the spermatheca, and the 7.5-μm-long metaphase spindle remained at the cortex for 10 min before initiating its shortening phase. (D) In *unc-116(RNAi)* embryos, the meiotic spindle did not initiate movement toward the cortex until the time that spindle shortening initiated. (E) In embryos arrested at metaphase I due to a temperature-sensitive APC mutant, *mat-2(ts)*, spindle shortening did not initiate but translocation to the cortex was normal. Thus, wild-type translocation is APC independent. (F) In *mat-2(ts); unc-116(RNAi)* double mutant embryos, the spindle did not shorten and never translocated to the cortex. Thus, the movement of *unc-116(RNAi)* spindles toward the cortex is APC dependent. (G and H) Fixed time point images of GFP-tubulin–labeled spindles in metaphase-arrested *mat-2(ts)* (G) or *mat-2(ts); unc-116(RNAi)* (H) worms. Bars, 10 μm.

period is clearly seen in Fig. 1 B from 0 to 6.0 min. These observations suggested that an early translocation mechanism that is activated while the zygote is in the spermatheca of wild-type worms is completely absent in *unc-116(RNAi)* worms and that a distinct mechanism is responsible for the late movement of *unc-116(RNAi)* spindles to the cortex.

Consistent with this hypothesis, the orientation of spindles moving toward the cortex was different between *unc-116(RNAi)* and wild-type spindles. In wild-type worms, 14/17 (82.4%) of the meiotic spindles approached the cortex in a sideways orientation (e.g., Fig. 1 A). After the prolonged stationary period, 10/12 (83.3%) *unc-116(RNAi)* spindles moved toward the cortex with one pole leading (e.g., Fig. 1 B). The velocity of late translocation in *unc-116(RNAi)* worms was also different than the velocity of early translocation in wild-type worms (Table I). Thus, *unc-116(RNAi)* worms appear to be completely defective in an early translocation mechanism but retain a distinct, late translocation mechanism.

The movement of *unc-116(RNAi)* spindles is mediated by a distinct, anaphase-promoting complex (APC)–dependent mechanism

If movement of *unc-116(RNAi)* spindles to the cortex is indeed due to a discrete, late mechanism, this should be revealed by distinct genetic requirements for the early and late mechanisms. In a previous study (Yang et al., 2003), we showed that wild-type spindle translocation is followed sequentially by spindle shortening, spindle rotation, and anaphase chromosome segregation. Depletion of APC subunits had no effect on spindle translocation but blocked spindle shortening and rotation (Fig. 1 E; Yang et al., 2003). These results indicated that spindle shortening is APC dependent, whereas early translocation is APC independent. To test whether or not the late translocation observed in *unc-116(RNAi)* embryos is APC dependent, we compared the kinetics of spindle shortening and spindle translocation in wild-type worms with those of worms depleted of UNC-116, the APC subunit, MAT-2, or both.

In 19/19 wild-type worms, spindles initiated translocation while the zygote was in the spermatheca and arrived at the cortex 7.2 ± 1.7 min before spindle shortening initiated (Fig. 1 C). However, in 9/9 *unc-116(RNAi)* time-lapse sequences, where the spindle was oriented such that both translocation and shortening could be measured, translocation initiated at the same time that spindle shortening initiated and spindles arrived at the cortex 3.6 ± 1.1 min after shortening started (Fig. 1 D). As previously reported for worms depleted of the FZY-1 subunit of the APC (Yang et al., 2003), spindle shortening was blocked in *mat-2 (ts)* worms at nonpermissive temperature but spindle translocation occurred with wild-type kinetics. (Fig. 1 E, $n = 5$). In 5/5 of *mat-2(ts); unc-116(RNAi)* double mutant worms, spindle length did not change and spindle translocation to the cortex was completed blocked (Fig. 1 F). The complete block to spindle translocation in *mat-2(ts); unc-116(RNAi)* double mutant worms was confirmed by single time point analysis (Fig. 1 H) to eliminate any contribution by photodamage. These results dem-

Table I. **Velocities of meiotic spindle movements**

	Wild type	*unc-116 (RNAi)*	*klc-1 (RNAi); klc-2 (RNAi)*	C10H11.10 *kca-1 (RNAi)*	*unc-116 (sb79rh24)*
Movies	27	15	4	11	5
Time from GVBD[a] to pronucleus formation (min)	42.2 ± 5.1	38.5 ± 5.0	39.4 ± 0.8	42.0 ± 5.7	39.0 ± 1.3
Diakinesis nuclear positioning (dorsal-ventral axis)	46%	47%	ND	ND	ND
Meiosis I					
Maximum spindle length (μm)	8.0 ± 0.7	8.2 ± 0.7	8.5 ± 0.3	8.0 ± 0.4	8.1 ± 0.6
Maximum spindle width (μm)	6.3 ± 0.5	6.4 ± 0.5	7.2 ± 0.6	5.9 ± 0.4	6.1 ± 0.3
Distance from spindle to cortex after exit from spermatheca (μm)	2.3 ± 2.1	7.2 ± 0.1	5.4 ± 1.6	6.8 ± 1.5	5.3 ± 1.8
Timing of cortical contact after exit from spermatheca (min)	1.0 ± 0.7	8.3 ± 2.2	10.9 ± 4.5	10.0 ± 2.0	9.2 ± 1.5
Translocation rate (μm/min)	0.9 ± 0.4	3.5 ± 1.2 ($P < 0.001$)	3.2 ± 0.6	4.6 ± 1.8	2.0 ± 0.8
Time from GVBD to first spindle shortening (min)	18.7 ± 3.3	13.3 ± 1.9	17.8 ± 6.1	16.9 ± 2.0	15.2 ± 4.2
Shortening rate[b] (μm/min)	0.8 ± 0.2	1.2 ± 0.3	0.9 ± 0.2	1.2 ± 0.4	0.7 ± 0.2
Chromosome segregation rate[c] (μm/min)	0.7 ± 0.1 ($n = 11$)	1.1 ± 0.5 ($n = 5$)	ND	ND	ND
Meiosis II					
Maximum spindle length (μm)	6.3 ± 0.5	6.6 ± 0.4	6.7 ± 0.5	6.7 ± 0.9	6.5 ± 0.5
Maximum spindle width (μm)	4.9 ± 0.5	5.0 ± 0.6	4.0 ± 0.5	4.7 ± 0.5	5.0 ± 0.4
Distance to cortex after spindle assembly (μm)	0.9 ± 0.4	3.4 ± 1.2	2.1 ± 0.5	2.9 ± 1.3	4.0 ± 2.6
Timing of cortical contact after spindle assembly (min)	0.7 ± 0.4	6.0 ± 0.9	7.2 ± 1.8	8.5 ± 2.5	7.1 ± 1.0
Translocation rate (μm/min)	1.1 ± 0.6	4.6 ± 1.5	2.7 ± 2.0	4.7 ± 1.1	4.8 ± 2.5
Time from GVBD to second spindle shortening (min)	33.5 ± 2.8	27.6 ± 3.1	30.1 ± 1.1	32.1 ± 4.5	28.3 ± 1.5
Shortening rate[b] (μm/min)	0.8 ± 0.2	1.5 ± 0.4	1.5 ± 0.6	1.3 ± 0.4	1.3 ± 0.4
Chromosome segregation rate[c] (μm/min)	1.1 ± 0.6 ($n = 11$)	1.2 ± 0.6 ($n = 5$)	ND	ND	ND

[a]GVBD denotes germinal vesicle breakdown or nuclear envelope breakdown.
[b]The change in pole–pole spindle length over time.
[c]The change in distance between two sets of GFP-histone–labeled chromosomes over time.

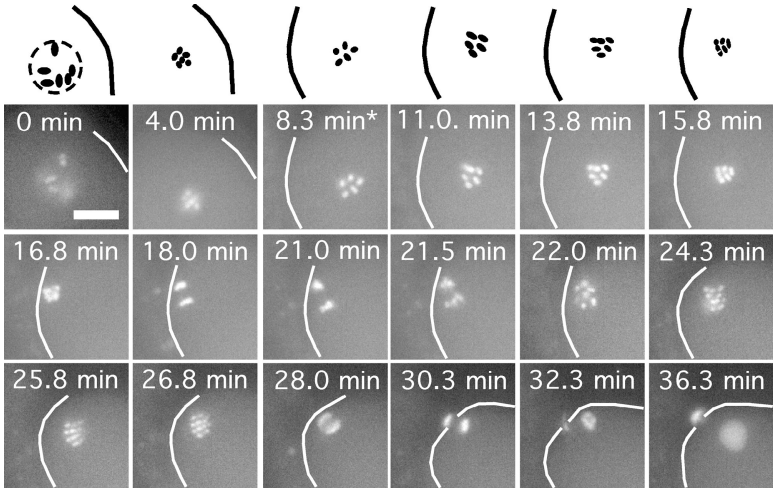

Figure 2. **Polar body formation in an *unc-116(RNAi)* embryo.** Images of GFP-histone H2b fluorescence within a meiotic embryo are shown from a representative time-lapse sequence of an *unc-116(RNAi)* worm. The cortex has been highlighted in each image and drawings corresponding to the top row of images are included for clarity. Note that anaphase of meiosis I is successful (18 min) but the chromosomes that should have been sequestered in a polar body snap back to produce a meiosis II spindle with 12 rather than 6 chromosomes (22.0–24.3 min). Anaphase of meiosis II was also successful (30.3 min), and the chromosomes segregated into the cortex were successfully sequestered in a polar body (36.3 min). Asterisk indicates exit of the zygote from the spermatheca into the uterus. Bar, 10 μm.

onstrated that the late spindle translocation observed in *unc-116(RNAi)* worms is APC dependent and kinesin-1 independent whereas the early translocation mechanism observed in wild-type worms is APC independent and kinesin-1 dependent.

UNC-116 is not required for other aspects of meiosis

We previously demonstrated that both tubulin and the katanin orthologue MEI-1 are required for meiotic spindle translocation (Yang et al., 2003). In both of these cases, however, spindle structure was severely perturbed, making it impossible to discern if MEI-1 is directly involved in spindle translocation or if normal spindle architecture is required for translocation. In contrast, *unc-116(RNAi)* meiotic spindles observed by GFP-tubulin fluorescence had a wild-type structure (Fig. 1, B and H). These spindles had wild-type length and width (Table I), exhibited normal anaphase chromosome segregation (Fig. 2 and Table I), and shortened with normal kinetics (Table I and Fig. 1 D). These results indicate that UNC-116 is primarily (if not exclusively) required in the early embryo for meiotic spindle translocation.

UNC-116 is also essential for cortical positioning of the meiosis II spindle

The early, APC-independent and UNC-116–dependent translocation mechanism might be activated only transiently or it might be active throughout meiosis. Careful observation of meiosis II spindles in *unc-116(RNAi)* worms indicated that the UNC-116–dependent mechanism continues to be active during meiosis II. Whereas the meiosis II spindle in a wild-type embryo is already extremely close to the cortex as it assembles (Fig. 1 C and Video 1, available at http://www.jcb.org/cgi/content/full/jcb.200411132/DC1), the meiosis II spindle in an *unc-116 (RNAi)* embryos remains stationary several micrometers from the cortex (Fig. 1 D, Table I, and Video 2, available at http://www.jcb.org/cgi/content/full/jcb.200411132/DC1) until the meiosis II spindle begins to shorten. Meiosis II spindles in *unc-116(RNAi)* embryos also move in a pole-first orientation with a high velocity (Table I). These results indicate that the force generated on the spindle by wild-type UNC-116 is active throughout meiosis I and meiosis II. It is likely that the same APC-dependent mechanism that mediates movement of meiosis I spindles to the cortex in the absence of UNC-116 also mediates the delayed translocation of meiosis II spindles to the cortex.

UNC-116 is essential maternally because it is required for polar body formation

To determine the consequences of delayed spindle translocation, we filmed GFP-histone in *unc-116(RNAi*) worms to track chromosome movements during meiosis. In 5/5 cases where delayed spindle translocation was observed, anaphase chromosome segregation occurred normally with one set of chromosomes being pushed into the cortex during both anaphase I and II (Fig. 2). However, failures in polar body formation during meiosis I, meiosis II, or both were frequently observed. In the example shown in Fig. 2, chromosomes that segregated into the cortex at meiosis I (21 min) collapsed back into the embryo so that 12 rather than 6 chromosomes were present in the meiosis II spindle (24.3 min). In this example, meiosis II polar body formation was successful (36.3 min). In 60% of GFP-histone *unc-116(RNAi)* movies, one or both polar bodies failed to form, even though anaphase occurred at the cortex. In contrast, both polar bodies formed successfully in 100% of GFP-histone wild-type time-lapse sequences ($n = 11$). To eliminate any contribution from photodamage, polar body number was also scored by fixed time point analysis. A failure to form one or both polar bodies was observed in 67% of *unc-116(RNAi)* embryos compared with 5% of wild-type embryos (see Table III). A failure to form one or both polar bodies should result in embryos that are triploid or pentaploid. Whereas triploid worms can be viable (Madl and Herman, 1979), pentaploidy would be expected to cause embryonic lethality later in development. Indeed, 67% embryonic lethality was observed among embryos laid by *unc-116(RNAi)* worms (Table II). These results indicate that UNC-116 and the early spindle translocation pathway are required for meiotic cytokinesis, even though the spindles always achieve perpendicular cortical contact eventually.

Because kinesin-1 has never been found to be essential for cell division in other species (Wright et al., 1993; Brendza

Table II. **Embryonic lethality due to depletion of UNC-116 and associated proteins**

Genotype	Embryonic lethality	Brood size
	%	
wild type	3.3 ± 4 (9,999/95)	174.4
wild type + males	2.6 ± 0.4 (4,509/28)	241.6
unc-116(RNAi)	66.9 ± 19 (2,230/45)	71.8
unc-116(RNAi) + males	65.3 ± 26 (1,904/16)	161.6
unc-116(rh24,sb79)	27.8 ± 9 (1,099/23)	57.5
unc-116(rh24,sb79) + males	24.0 ± 9 (800/24)	40.4
unc-116(rh24,sb79, RNAi)	72.5 ± 6 (560/24)	28.5
unc-116(rh24,sb79, RNAi) + males	58.2 ± 11 (756/23)	39.2
klc-1(RNAi)	16.4 (785/10)	156.1
klc-1(RNAi) + males	11.7 (725/9)	132.2
klc-2(RNAi)	1.7 (879/9)	166.1
klc-2(RNAi) + males	4.3 (836/7)	155.3
klc-1(RNAi); klc-2(RNAi)	65.8 (912/17)	113.4
klc-1(RNAi); klc-2(RNAi) + males	64.6 (1,584/10)	221.6
C10H11.10/*kca-1(RNAi)*	89.2 ± 9 (1,719/54)	73.4
C10H11.10/*kca-1(RNAi)* + males	69.0 ± 20 (2,660/30)	121.7

Embryonic lethality is the percentage of eggs that did not hatch within 12 h. Numbers in parentheses indicate the number of embryos counted/number of worms tested by RNAi soaking. + males indicates that male worms were added to provide wild-type sperm. Brood size is the average number of eggs laid by a single worm in 48 h. Wild-type is the GFP-tubulin–expressing strain WH204.

et al., 2000) and because RNAi can result in depletion of homologous mRNAs, we wished to confirm that the spindle translocation defect and the maternal-effect embryonic lethality were actually due to a reduction in the amount of UNC-116 activity. Therefore, we analyzed a recessive, loss-of-function allele of *unc-116, unc-116(rh24sb79)* (see Materials and methods). Homozygous *unc-116(rh24sb79)* worms are extremely uncoordinated and exhibited 28% maternal-effect embryonic lethality at 25°C compared with 67% for *unc-116(RNAi)* (Table II), indicating that *unc-116(rh24sb79)* worms retain more UNC-116 activity than *unc-116(RNAi)* worms. Western blotting with an UNC-116–specific antibody revealed more intact UNC-116 polypeptide in *unc-116 (rh24sb79)* adult hermaphrodites (Fig. S1, lane 8, available at http://www.jcb.org/cgi/content/full/jcb.200411132/DC1) than in *unc-116(RNAi)* adults (Fig. S1, lane 2), confirming the hypomorphic classification of this allele.

Consistent with the hypomorphic nature of the *rh24sb79* allele, time-lapse imaging of GFP-tubulin *unc-116(rh24sb79)* worms revealed a block in preanaphase meiotic spindle translocation in only 7/14 worms (Fig. S2, available at http://www.jcb.org/cgi/content/full/jcb.200411132/DC1) versus 15/19 for *unc-116(RNAi)*. Significantly, the combination of RNAi and this loss-of-function allele did not increase the level of embryonic lethality beyond that of *unc-116(RNAi)* alone (Table II). This finding strongly suggests that *unc-116(RNAi)* indeed represents the *unc-116(null)* embryonic phenotype. We conclude that both the spindle translocation defect and the maternal-effect embryonic lethality observed in *unc-116(RNAi)* worms is in fact due to a severe reduction (if not total elimination) of UNC-116 activity.

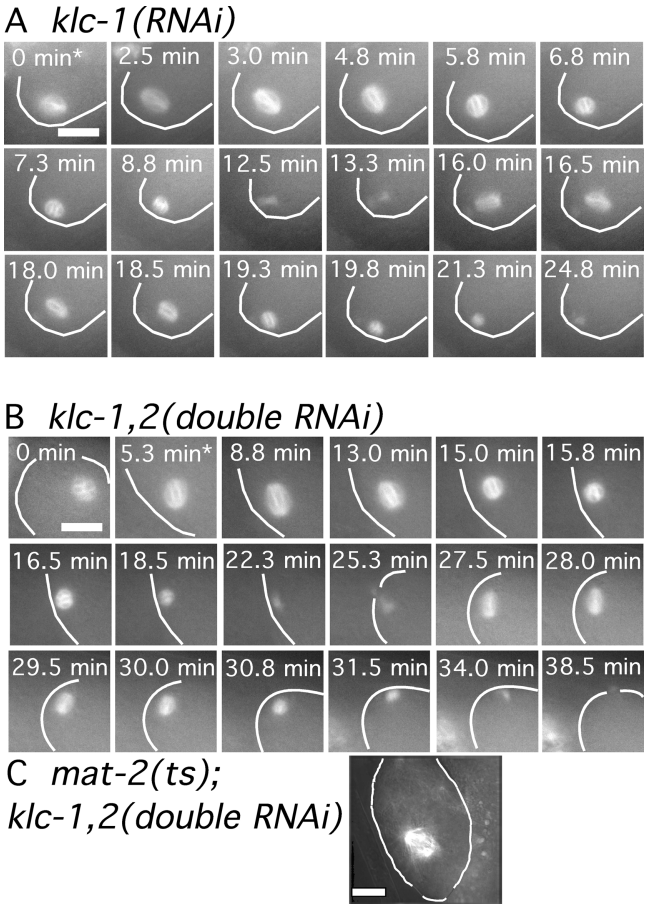

Figure 3. **Kinesin light chains are required for normal translocation of the meiotic spindle to the cortex.** Images of GFP-tubulin fluorescence are shown from representative time-lapse sequences of a meiotic embryo within a *klc-1(RNAi)* worm (A) and a *klc-1(RNAi); klc-2(RNAi)* worm (B). The cell cortex was highlighted in each image for clarity. In both cases, the meiosis I and II spindles do not move toward the cortex until after spindle shortening has initiated. Asterisks indicate exit from the spermatheca. (C) Fixed time point image of a *mat-2(ts); klc-1(RNAi); klc-2(RNAi)* triple mutant worm shows a meiotic spindle arrested far from the cortex. Bars, 10 μm.

The kinesin light chains KLC-1 and -2 are required for early spindle translocation

Kinesin-1 purified from a variety of species, including *C. elegans*, consists of a tetramer with two heavy chain and two light chain subunits (Vale et al., 1985; Saxton et al., 1988; Signor et al., 1999). To test whether or not early meiotic spindle translocation depends on a kinesin-1 heavy chain/light chain complex, we acquired GFP-tubulin time-lapse sequences from worms treated with dsRNA corresponding to either of the *C. elegans* kinesin light chain homologues, KLC-1 or KLC-2. A block to early spindle translocation was observed in 3/6 *klc-1(RNAi)* worms, 2/7 *klc-2(RNAi)* worms, and 4/5 doubly treated *klc-1(RNAi); klc-2(RNAi)* worms (Fig. 3, A and B; and Table I). In addition, depletion of kinesin light chains in metaphase-arrested *mat-2(ts)* embryos resulted in spindles arrested far from the cortex (Fig. 3 C). Thus, the phenotype of *klc-1(RNAi)* or *klc-2(RNAi)* worms was qualitatively the same, but quantitatively weaker, than the phenotype of *unc-116(RNAi)* embryos. Western blots of *klc-2(RNAi)* worms probed with a KLC-2–specific antibody revealed that considerable KLC-2 protein

Table III. **Polar body formation**

Genotype	Fraction of embryos with one or no polar bodies	Number of embryos scored
	%	
wild type	5.6	54
unc-116(RNAi)	67.7	31
klc-1(RNAi)	38.5	26
klc-2(RNAi)	28.1	31
klc-1(RNAi); klc-2(RNAi)	55.6	27
C10H11.10/*kca-1(RNAi)*	72.7	44

Hermaphrodites expressing GFP-histone were soaked in the indicated dsRNAs for 16 h at 25°C, and polar bodies were counted in pronuclear stage embryos 24 h after returning the worms to bacteria.

product remains in these worms (Fig. S1). Thus the weaker phenotypes observed were at least in part due to the incomplete effectiveness of the RNAi. Simultaneous treatment of worms with dsRNAs corresponding to both light chains (*klc-1(RNAi); klc-2(RNAi)*) resulted in embryonic lethality (Table II), polar body defects (Table III), and translocation defects that were quantitatively similar to *unc-116(RNAi)* worms. These results indicate that the two kinesin light chains act redundantly and that a complex of kinesin heavy and light chains is essential for the preanaphase translocation of the meiotic spindle.

KCA-1 mediates UNC-116–dependent spindle translocation

In neurons, a membrane-associated cargo-adaptor protein called *sunday driver* forms a bridge between kinesin light chains and vesicles transported during fast axonal transport (Bowman et al., 2000). To identify a possible cargo-adaptor protein linking KLC-1 or KLC-2 to the meiotic spindle, we used RNAi to screen putative kinesin light chain interacting proteins identified in a large scale yeast two hybrid study (Li et al., 2004). Treatment of *mat-2(ts)*, GFP-tubulin worms with dsRNA corresponding to one of these interacting gene products (C10H11.10), resulted in meiotic spindles that were far from the cortex of metaphase-arrested embryos (Fig. 4 B). In contrast, all meiotic spindles were at the cortex of metaphase-arrested embryos of *mat-2(ts)*, GFP-tubulin worms treated with other dsRNAs (unpublished data). Time-lapse imaging of GFP-tubulin in 11/11 C10H11.10(RNAi) single mutant worms revealed a block in preanaphase spindle translocation identical to that observed in *unc-116(RNAi)* or *klc-1(RNAi); klc-2(RNAi)* worms (Fig. 4 A and Table I). C10H11.10(RNAi) worms also exhibited embryonic lethality (Table II) and polar body defects (Table III) similar to those seen in *unc-116(RNAi)* and *klc-1(RNAi); klc-2(RNAi)* worms. These data are consistent with a mechanism in which the C10H11.10 gene product forms a bridge between the UNC-116–KLC-1,2 kinesin and the meiotic spindle. We have therefore given C10H11.10 the name *kca-1,* for kinesin cargo adaptor.

To directly demonstrate the existence of a protein complex containing UNC-116, KLC-2, and KCA-1, all three proteins were expressed as fusion proteins in *E. coli* and interactions were analyzed by glutathione Sepharose chromatography. As shown in Fig. 5 A (lane 10), a chitin-binding domain fusion to the UNC-116 stalk-tail domains stochiometrically copurified with a glutathione S–transferase fusion to KCA-1 only in the presence of 6his-KLC-2b. This experiment demonstrated that KLC-2b can either bind simultaneously to both UNC-116 and KCA-1 or that KLC-2b induces a conformational change that increases the affinity between UNC-116 and KCA-1. Similar experiments with KCA-1 deletion derivatives (Fig. 5 B) indicated that the NH_2-terminal 155 amino acids of KCA-1 contain the KLC-2 binding domain. This result implies that the COOH-terminal part of KCA-1 may bind to some spindle component to generate a bridge between UNC-116 and the meiotic spindle. KCA-1 has no homology with *sunday driver* or other known kinesin-associated proteins and thus represents a novel kinesin cargo adaptor.

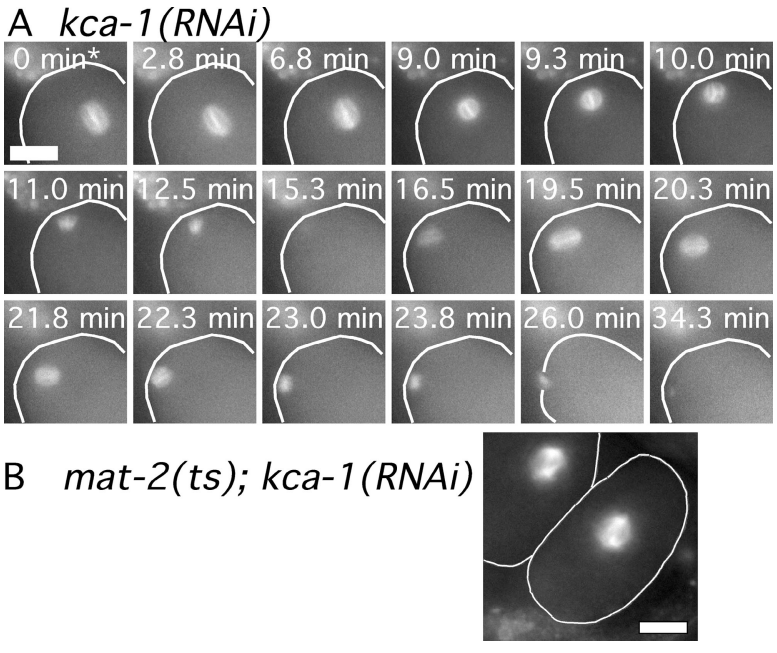

Figure 4. **C10H11.10/KCA-1 is required for normal translocation of the meiotic spindle to the cortex.** (A) Images of GFP-tubulin fluorescence are shown from a representative time-lapse sequence from a meiotic embryo within a *kca-1(RNAi)* worm. The cell cortex was highlighted in each image for clarity. The meiosis I and meiosis II spindles do not move toward the cortex until after spindle shortening has initiated. The asterisk indicates exit from the spermatheca. (B) Fixed time point image of *mat-2(ts); kca-1(RNAi)* worms shows a meiotic spindle arrested far from the cortex. Bars, 10 μm.

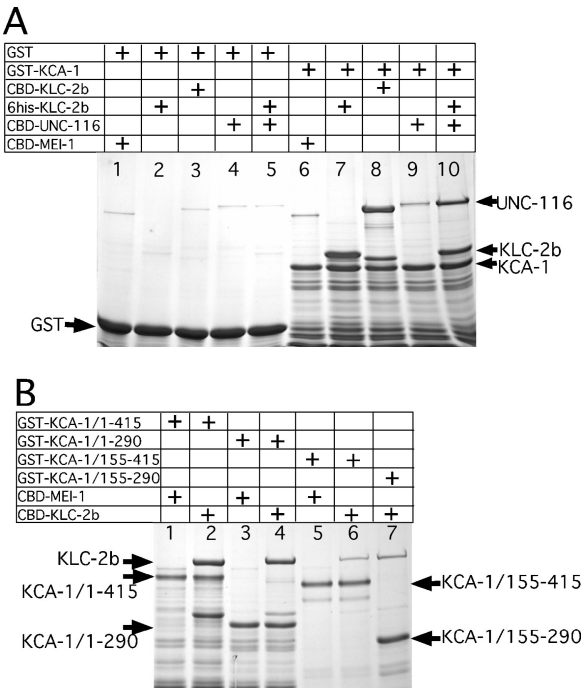

Figure 5. **In vitro reconstitution of a complex between kinesin heavy chain, kinesin light chain, and KCA-1.** (A) Glutathione Sepharose beads were coated either with glutathione S-transferase (GST; lanes 1–5) or a GST fusion with aa 1–290 of KCA-1 (GST-KCA-1; lanes 6–10). Coated beads were incubated with different chitin binding domain intein fusion proteins (CBD) and washed extensively, and the bound complexes were eluted with SDS, resolved by SDS-PAGE, and detected with Coomassie brilliant blue R staining. The negative control, CBD-MEI-1, did not bind to GST (lane 1) or KCA-1 (lane 6). In contrast, both a 6his-KLC-2b fusion (lanes 2 and 7) and a CBD-KLC-2b fusion (lanes 3 and 8) bound with a high stochiometry to KCA-1 but not to the GST control. CBD-UNC-116 (lanes 4 and 9) bound to KCA-1 with a low stochiometry, but significantly more CBD-UNC-116 associated with KCA-1 beads when 6his-KLC-2b was also present (lanes 5 and 10). This result indicates that KLC-2b can form a ternary complex with both UNC-116 and KCA-1. (B) Glutathione Sepharose beads were coated with GST fusions to different deletion derivatives of KCA-1 and incubated either with the negative control, CBD-MEI-1 (lanes 1, 3, and 5), or CBD-KLC-2b (lanes 2, 4, 6, and 7). Beads were washed extensively and bound complexes were eluted with SDS, resolved by SDS-PAGE, and detected with Coomassie brilliant blue R staining. A high stochiometry of CBD-KLC-2b associated with both aa 1–415 of KCA-1 (lane 2) and aa 1–290 (lane 4). In contrast, much less CBD-KLC-2b associated with KCA-1 aa 155–415 (lane 6) or 155–290 (lane 7). These results indicate that most of the binding to KLC-2b is mediated by the NH_2-terminal 155 aa of KCA-1. Note that all lanes containing CBD-KLC-2b also have a polypeptide corresponding to KLC-2b alone produced by spontaneous cleavage of the intein fusion. Also, KCA-1 derivatives that contain the COOH-terminal 125 aa migrate anomalously slowly relative to derivatives without this region.

Cytoplasmic dynein is not required for preanaphase spindle translocation

One hypothesis consistent with our results is that kinesin-1 transports the spindle on a subset of cytoplasmic microtubules that have plus ends oriented toward the cortex. An alternative model, suggested by work in *Aspergillus nidulans* (Zhang et al., 2003) and *D. melanogaster* (Brendza et al., 2002), is that UNC-116 is only required to localize the minus end–directed motor, cytoplasmic dynein. In this model, cytoplasmic dynein would be required to move the spindle on a subset of cytoplasmic microtubules that have minus ends oriented toward the cortex. Therefore, we tested if early meiotic spindle translocation is blocked when cytoplasmic dynein heavy chain, DHC-1, is depleted by RNAi. As previously reported (Gonczy et al., 1999), the strongest phenotype observed after prolonged treatment with *dhc-1* dsRNA was failure to ovulate mature oocytes. Shorter treatment of worms with *dhc-1*(RNAi) resulted in meiosis I spindles with a variety of structural defects. Some spindles were longer than wild-type spindles and had extremely pointed poles, whereas others were extremely disorganized. Time-lapse imaging of GFP-tubulin–labeled spindles under these weak *dhc-1(RNAi)* conditions revealed that 7/7 spindles arrived at the cortex either before or within 1.0 ± 0.4 min (1.0 ± 0.7 min in wild type) after exit from spermatheca (Fig. 6 A). At longer time points of *dhc-1* dsRNA treatment, before worms ceased to produce mature oocytes, multiple small diakinesis nuclei were observed in immature oocytes (Fig. 6 B). Time-lapse imaging of GFP-tubulin revealed that each of these nuclei gave rise to a spindle-like structure at germinal vesicle breakdown and that all of these structures were eventually associated with the cortex (Fig. 6 B, 30.5 min). Tracking the early movements of these spindles to determine the time of cortical contact, however, proved difficult and was not pursued. To determine whether or not the early, APC-independent translocation mechanism was functional in these *dhc-1(RNAi)* embryos, *mat-2(ts)*, GFP-tubulin worms, were treated with *dhc-1* dsRNA at 25°C so that metaphase-arrested meiotic embryos that were derived from oocytes with multiple germinal vesicles could be observed. The majority of meiotic spindles in these *mat-2(ts)*; *dhc-1(RNAi)* double mutant embryos were associated with the cortex just as in *mat-2(ts)* single mutants (Fig. 6 C). These results provide no indication of a role for cytoplasmic dynein in the early, APC-independent spindle translocation. Thus, UNC-116 appears to play a more direct role in early spindle translocation, possibly by transporting the spindle on cytoplasmic microtubules that are oriented with their plus ends toward the cortex. An obvious challenge is elucidating how the acentrosomal cytoplasmic microtubule array shown in Fig. 6 D can be organized to allow directional transport.

Discussion

Two redundant pathways can move *C. elegans* meiotic spindles to the cortex

Our results indicate that in *C. elegans* female meiotic spindles are positioned at the cell cortex by two sequential mechanisms, an early, kinesin-1–dependent pathway that moves spindles in a sideways orientation and a late, APC-dependent pathway that pulls the spindle toward the cortex with one pole leading (Fig. 7). Wild-type meiotic spindles begin kinesin-1–dependent movement toward the cortex as soon as they have assembled into bipolar structures, while the embryo is still inside the spermatheca. In the absence of kinesin-1, the meiosis I spindle is stationary in the cytoplasm during the 7-min period before spindle shortening begins. The spindle then suddenly moves to the cortex with one pole leading just after spindle shortening initiates. We propose that the sudden movement of *unc-116(RNAi)* spindles to the cortex is mediated by the same mechanism as wild-type spindle rotation and that it is mediated

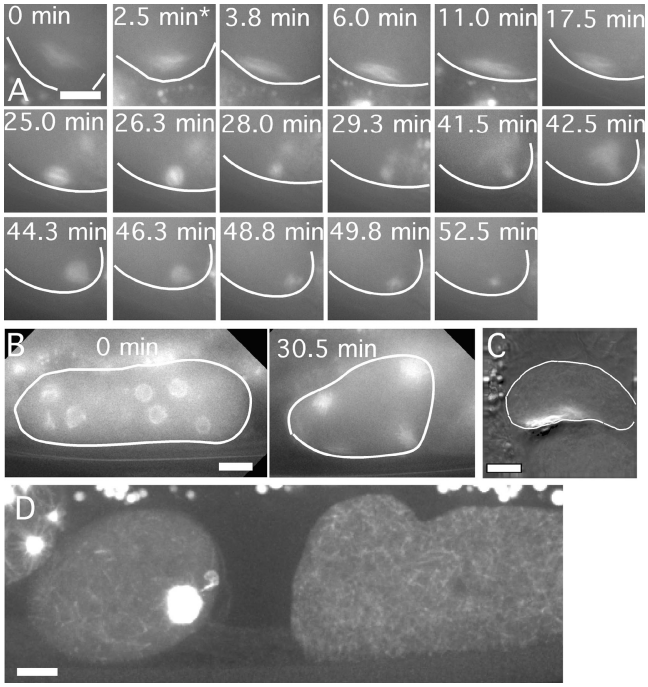

Figure 6. **Dynein heavy chain is not required for preanaphase spindle translocation.** Images of GFP-tubulin fluorescence within a meiotic embryo are shown from representative time-lapse sequences from *dhc-1(RNAi)* worms. The cell cortex was highlighted in each image for clarity. (A) Worms observed at short time points after soaking in *dhc-1* dsRNA exhibited bipolar meiotic spindles that translocated to the cortex immediately after exit from the spermatheca (asterisk), long before initiation of spindle shortening. Two female pronuclei formed at the end of this sequence and these pronuclei did not migrate toward the male pronucleus as reported by Gonczy et al. (1999). (B) Worms observed at longer time points after soaking in *dhc-1* dsRNA had multiple germinal vesicles in the diakinesis-stage oocytes before maturation. The 0 min image shows an oocyte during germinal vesicle breakdown as GFP-tubulin is polymerizing within each fenestrated nucleus. All of these spindles ended up at the cortex (30.5 min) after coalescing into a smaller number of spindles. (C) Fixed time point image of a *mat-2(ts); dhc-1(RNAi)* worm shows a disorganized spindle that is tightly associated with the cortex. (D) Maximum intensity projection of a z-stack of spinning disk confocal images of GFP-tubulin fluorescence in a living, wild-type worm. Brightness has been adjusted to reveal the cytoplasmic microtubule array in the meiotic embryo on the left and the immature oocyte on the right. The black region in between is the spermatheca. Bars, 10 μm.

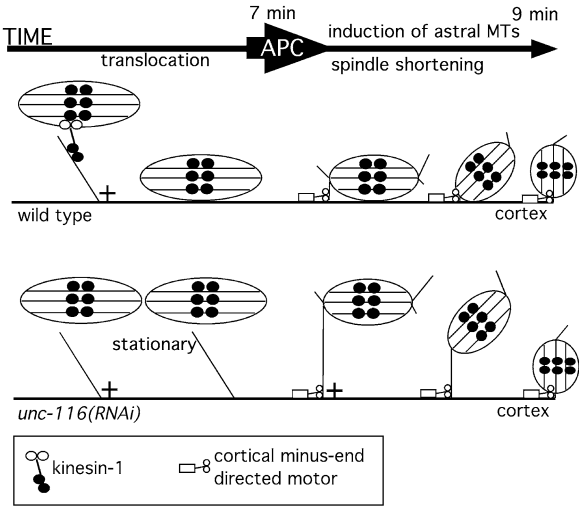

Figure 7. **Model for the sequential action of the early, UNC-116–dependent spindle translocation pathway and the late, APC-dependent pathway.** In wild-type worms, UNC-116 moves the spindle on cytoplasmic microtubules toward the cortex. At the APC-dependent metaphase–anaphase transition, astral microtubules extend from one pole and mediate pulling forces. In wild-type embryos, this APC-dependent cortical pulling results in rotation. In *unc-116(RNAi)* embryos, the same force generates translocation with one pole leading.

by microtubules extending from one spindle pole to the cortex. In wild-type spindles, pulling a spindle pole for only 2 μm would generate a rotation, whereas in *unc-116(RNAi)* spindles, the same pulling force would generate a pole-first translocation over a distance of 7 μm (Fig. 7). This model is supported by the finding that both wild-type spindle rotation and UNC-116–independent translocation are blocked when the APC is inhibited. The model is also supported by the finding that both wild-type rotation and UNC-116–independent translocation occur just after initiation of APC-dependent spindle shortening. Finally, UNC-116–dependent translocation seen in wild-type worms occurs with the spindle oriented parallel to the cortex, whereas UNC-116–independent translocation occurs with one pole leading. Direct visualization of microtubules extending from one pole to the cortex has thus far been stymied by the presence of a microtubule meshwork that fills the entire meiotic embryo. Two successive and partially redundant pathways also mediate mitotic spindle positioning in budding yeast (Schuyler and Pellman, 2001).

The relationship between spindle translocation and polar body formation

Both time-lapse imaging and fixed time point analysis revealed that one or both polar bodies failed to form in 67% of *unc-116(RNAi)* embryos. This finding could indicate that UNC-116 has a separate role in polar body formation. Alternatively, the delayed arrival of *unc-116(RNAi)* spindles at the cortex might sometimes be "just in time" and sometimes be "just too late" to induce polar body formation. We favor the latter explanation. The finding that treatment of *unc-116(rh24sb79)* mutant worms with *unc-116* dsRNA did not increase embryonic lethality beyond the 67% seen in *unc-116(RNAi)* alone indicates that 67% embryonic lethality is the null embryonic phenotype for *unc-116*. Thus, in 33% of *unc-116(RNAi)* embryos, both polar bodies form in the absence of UNC-116 activity. Examples of this successful polar body formation were observed in time-lapse sequences where early spindle translocation was completely blocked, and the spindle reached the cortex by the late, pole-first mechanism. These results suggest that even in the complete absence of maternal UNC-116, the late, APC-dependent mechanism can sometimes move the spindle to the cortex just in time for polar body induction.

KCA-1 as a novel cargo adaptor for the meiotic spindle

We showed that the previously uncharacterized gene product C10H11.10/KCA-1 can form a stochiometric protein complex with the kinesin light chain KLC-2b and the kinesin heavy chain UNC-116 in vitro. Furthermore, *kca-1(RNAi)* yields the same phenotype as depletion of heavy chain or depletion of

both light chains. These results indicate that KCA-1 may be the cargo adaptor that allows UNC-116 to form transient attachments to the meiotic spindle. The *Caenorhabditis briggsae* predicted gene CBG03328 (Wormbase) exhibits 40% amino acid identity over its entire length with KCA-1, but no homologues outside of nematodes or obvious sequence motifs are apparent. In the *C. elegans* global yeast two-hybrid analysis of Li et al. (2004), KCA-1 interacted only with the kinesin light chains KLC-1 and KLC-2 and with HPL-2. HPL-2 is one of two *C. elegans* orthologues of heterochromatin binding protein 1, a highly conserved component of pericentric heterochromatin (Couteau et al., 2002). If KCA-1 and HPL-2 interact in vivo, this interaction would complete a physical bridge between UNC-116 and the meiotic chromosomes. In this model, UNC-116 would transport meiotic chromosomes toward the cell cortex along cytoplasmic microtubules and the spindle would be dragged along with the chromosomes. This hypothetical mechanism would be consistent with the sideways orientation of spindles during wild-type spindle translocation.

Although our data support a model in which kinesin-1 transports the spindle along cytoplasmic microtubules, there is a 120-fold difference between the gliding velocity of purified *C. elegans* kinesin-1 (2 μm/s; Signor et al., 1999) and spindle translocation velocity (1 μm/min). The unexpectedly slow translocation might be explained if the UNC-116–KLC–KCA-1 complex actually acts indirectly, perhaps by organizing the cytoplasmic microtubule array. However, we favor a model in which translocation is slowed by opposing forces from kinesin-1 molecules that attempt to transport the spindle on microtubules with plus ends oriented away from the cortex.

Acentriolar spindles are positioned by unique mechanisms

Positioning of female meiotic spindles at the oocyte cortex is observed in all animal species, resulting in highly asymmetric divisions giving rise to small polar bodies and one large oocyte in most species. In some organisms such as *Chaetopterus variopedatus* (Lutz et al., 1988), *Spisula solidissima* (Palazzo et al., 1992), and starfish (Hamaguchi, 2001; Zhang et al., 2004), female meiotic spindles have robust astral microtubule arrays nucleated by centriole-containing centrosomes. In these species, it is likely that motor proteins associated with the cortex generate pulling forces on astral microtubules by the same mechanisms proposed for mitotic spindles in many species (Gonczy, 2002; Sheeman et al., 2003). In contrast, female meiotic spindles from organisms such as nematodes (Albertson and Thomson, 1993) and humans (Sathananthan, 1997) do not have centrioles and astral microtubule arrays are not apparent. It is reasonable to speculate that novel spindle positioning mechanisms have evolved to move acentriolar, anastral spindles to the oocyte cortex. Indeed, amphibian oocytes assemble a completely novel structure called the transient microtubule array that mediates movement of chromosomes to the cortex before a bipolar spindle is assembled (Becker et al., 2003). The genetic requirements for cortical translocation of preassembled, acentriolar meiotic spindles have been reported only for mouse (Verlhac et al., 2000) and *C. elegans* (Yang et al., 2003; this study), and these studies reveal apparently distinct requirements. Mouse meiotic chromosomes translocate to the cortex in the absence of microtubules using an actin-dependent mechanism, suggesting that the spindle is dragged along with the chromosomes (Verlhac et al., 2000). In contrast, movement of *C. elegans* meiotic chromosomes to the oocyte cortex is completely dependent on microtubules and apparently does not require F-actin (Yang et al., 2003). If the interaction between the *C. elegans* heterochromatin protein HPL-2 and the kinesin cargo adaptor KCA-1 occurs in vivo, then kinesin-1 may transport meiotic chromosomes, dragging the spindle along with the chromosomes. In this case, mice and worms would be using identical mechanisms mediated by different molecules.

Materials and methods

C. elegans strains

In this study, wild type indicates the integrated GFP-tubulin strain WH204 (Strome et al., 2001) or the integrated GFP-histone H2b strain AZ212 (Praitis et al., 2001), both of which are derived from N2. The integrated GFP-tubulin from WH204 was introduced into strains carrying *mat-2(ax76)*, *mat-2(ax102)*, or *unc-116(rh24sb79)* through crosses. *mat-2* strains were obtained from D. Shakes (College of William and Mary, Williamsburg, VA).

In utero filming

Adult hermaphrodites were anesthetized with tricaine/tetramisole and mounted between a coverslip and a thin agarose pad as described previously (Yang et al., 2003). Stage temperature was 22–24°C. Images were acquired at 15-s intervals on an upright microscope (model Microphot SA; Nikon) using a 60× PlanApo 1.4 objective and a Photometrics Quantix/KAF1400 camera (Roper Scientific). Illumination from an HBO100 light source was shuttered with a Uniblitz shutter. Time-lapse acquisition was controlled with IP Lab Spectrum software (Scanalytics). Quantitative analysis of translocation velocities was also performed with IP Lab Spectrum.

RNAi by soaking

The cDNA inserts of plasmid cDNA clones were amplified by PCR using one primer with a 5′ T7 promoter extension and a second primer with a 5′ T3 promoter extension. Linear PCR products were concentrated using spin columns (QIAGEN) and used as templates in separate T3 and T7 RNA polymerase transcription reactions (MegaScript T7 or T3 Kit; Ambion). After treatment with DNase I, RNAs were purified by LiCl precipitation and annealed. 40–50 L4 worms were soaked in 10 μl of 1 mg/ml dsRNA dissolved in 66 mM K-PO_4 and 10 mM K-citrate, pH 7.5, in a humidified chamber for 16 h at 25°C and then transferred to OP50-seeded plates to recover for 24 h before filming or lethality scoring. The following cDNA clones were used: KLC-1-yk1256g06, KLC-2-yk1323f03, C10H11.10-yk442h9, and UNC-116-yk255a4 (all obtained from Y. Kohara, National Institute of Genetics, Mishima, Japan). C10H11.10 was initially identified using RNAi by feeding with clone I-2I09 from the genomic RNAi feeding library (MRC Gene Service; Kamath et al., 2003).

Antibody generation

Rabbits were immunized with inclusion bodies composed of 6his-UNC-116 stalk tail or 6his-KLC-2b. UNC-116– or KLC-2–specific antibodies were bound to 6his-UNC-116 or 6his-KLC-2b immobilized on nitrocellulose strips and eluted with 200 mM glycine, pH 2.4, before neutralization with Tris-Cl, pH 8.0.

Protein interaction experiments

Different fragments of KCA-1 were PCR amplified from the yk624e12 cDNA clone. In the amino acid numbering shown in Fig. 5, 1 corresponds to a methionine that is 43 aa downstream from the predicted start codon in Wormbase. These fragments were cloned into pET41a (Novagen), expressed in BL21(DE3) *E. coli*, and purified by Ni^{2+} chelate chromatography via the 6his tag on the GST encoded by pET41a. Full-length KLC-2b was PCR amplified from yk886b10 and cloned into pET28a (Novagen) for expression of 6his-KLC-2b and into pTYB12 (New England Biolabs, Inc.) for expression of CBD-KLC-2b. The COOH-terminal 442 aa of UNC-116 were PCR amplified from yk859d09 and cloned into pTYB12. Full-

length MEI-1 was also PCR amplified and cloned into pTYB12. 6his-KLC-2b was purified by Ni^{2+} chelate chromatography after expression in *E. coli*. CBD-KLC-2b, CBD-UNC-116, and CBD-MEI-1 were expressed in *E. coli*, and high speed supernatants from microfluidized extracts were used directly in the binding assays without further purification after normalizing to equal concentrations of CBD fusion protein. 50 μl of glutathione Sepharose beads were incubated with an excess of GST-fusion protein for 1 h, and then washed extensively. Coated beads were incubated with 1 ml of *E. coli* lysate containing the appropriate CBD fusion and 25 mM Tris 8.0, 1 M NaCl, 0.1% Triton X-100, and 5% glycerol for 2 h at 22°C with constant rocking. After extensive washing with the same buffer, bound complexes were eluted with SDS-Laemmli buffer.

Isolation of *unc-116(rh24sb79)*

To identify a loss-of-function allele of *unc-116*, we reverted the gain-of-function properties of *unc-116(rh24)*. These were isolated as intragenic revertants that blocked the temperature-sensitive enhancement between *rh24/+* and *mei-1(ct46ts)/+*. Both *unc-116(rh24)* and *mei-1(ct46ts)/+* result in small, misoriented first cleavage spindles. At 20°C, *rh24/+* hermaphrodites segregate 12% dead embryos, 78% are lethal from *mei-1(ct46ts)/+* animals, whereas 99.5% of the embryos from the double mutant *rh24/+; mei-1(ct46ts)/+* fail to hatch. Replacing *rh24* with a chromosomal deficiency of the region in *nDf20/+; ct46ts/+* hermaphrodites produces 82% unhatched embryos, very close to the level seen with *ct46ts)/+* alone (all reported values are corrected for the lethality stemming from *nDf20* by itself). This finding indicates that *unc-116(rh24)* is a gain-of-function allele and that an *unc-116(null)/+* revertant could be isolated in this background.

The strain *mei-1(ct46ts) unc-29(e1072)/unc-13(e1091) daf-8(e1393) lin-11(n566) I; unc-116(rh24) dpy-17(e164)/qC1 III* was mutagenized with EMS and grown at 15°C (where 85% of the embryos are dead). When the oldest F_1 animals reached the last larval stage (L4), the plates were shifted to 20°C. A total of 7,200 F_1 progeny were shifted, of which 1/4 (1,800) were the relevant *rh24/+; mei-1(ct46ts)/+* genotype. Six plates produced an F_2 generation, indicating the presence an F_1 animal with a suppressor. One of these contained *sb79*, which is tightly linked to the original *rh24* mutation. Three-factor mapping indicated that *sb79* is <0.12 cM from *rh24*, consistent with an intragenic event (as confirmed by sequencing). The other five suppressors were linked to chromosome I and are likely alleles of *mei-1* and/or *mei-2*, which mutate to dominant suppressors of *ct46* at a high rate (Mains et al., 1990).

rh24sb79 behaves as a strong loss-of-function but not a null allele. *unc-116(rh24sb79)/+; mei-1(ct46ts)/+* showed about the same level of lethality at 20°C as *mei-1(ct46ts)/+* (70 vs. 78%), indicating that the enhancement of *mei-1* was completely lost by *rh24sb79*. Similar results were seen for mutations of two other genes, *mel-26(ct61)* and *zyg-9(b244)*, which are also strongly enhanced by *rh24* but not by *rh24sb79*. Although the lethality of *rh24/+* is semidominant, showing 26% unhatched embryos at 25°C, *rh24sb79/+* segregated only 1.2% dead embryos. Together, the aforementioned data indicate that *rh24sb79* is a strong loss-of-function mutation. However, it is not null because its behavior, when heterozygous with *rh24*, differs from that of a deficiency. Although the lethality of *rh24/nDf20* at 25°C was 87%, the value was 48% for *rh24/rh24sb79*. This finding indicates that *rh24sb79* has some *unc-116(+)* activity.

Online supplemental material

Video 1 corresponds to Fig. 1 A and Video 2 corresponds to Fig. 1 B. Fig. S1 shows anti–UNC-116 and anti–KLC-2 immunoblots of dsRNA-treated worms. Fig. S2 shows the spindle translocation defect in *unc-116(rh24sb79)*. Online supplemental material is available at http://www.jcb.org/cgi/content/full/jcb.200411132/DC1.

We thank Diane Shakes for *mat-2* strains, Yuji Kohara for cDNA clones, and Danielle Thierry-Mieg for communication of results prior to publication. We thank Lesilee Rose for advice and use of facilities throughout this work.

This work was supported by a grant from the University of California Cancer Research Coordinating Committee. P.E. Mains was supported by grants from the Canadian Institutes of Health Research and the Alberta Foundation for Medical Research.

Submitted: 22 November 2004
Accepted: 22 March 2005

References

Albertson, D.G., and J.N. Thomson. 1993. Segregation of holocentric chromosomes at meiosis in the nematode, *Caenorhabditis elegans*. *Chromosome Res.* 1:15–26.

Becker, B.E., S.J. Romney, and D.L. Gard. 2003. XMAP215, XKCM1, NuMA, and cytoplasmic dynein are required for the assembly and organization of the transient microtubule array during the maturation of *Xenopus* oocytes. *Dev. Biol.* 261:488–505.

Bowman, A.B., A. Kamal, B.W. Ritchings, A.V. Philp, M. McGrail, J.G. Gindhart, and L.S. Goldstein. 2000. Kinesin-dependent axonal transport is mediated by the sunday driver (SYD) protein. *Cell.* 103:583–594.

Brendza, R.P., K.B. Sheehan, F.R. Turner, and W.M. Saxton. 2000. Clonal tests of conventional kinesin function during cell proliferation and differentiation. *Mol. Biol. Cell.* 11:1329–1343.

Brendza, R.P., L.R. Serbus, W.M. Saxton, and J.B. Duffy. 2002. Posterior localization of dynein and dorsal-ventral axis formation depend on kinesin in *Drosophila* oocytes. *Curr. Biol.* 12:1541–1545.

Cha, B.J., B.S. Koppetsch, and W.E. Theurkauf. 2001. In vivo analysis of *Drosophila bicoid* mRNA localization reveals a novel microtubule-dependent axis specification pathway. *Cell.* 106:35–46.

Couteau, F., F. Guerry, F. Muller, and F. Palladino. 2002. A heterochromatin protein 1 homologue in *Caenorhabditis elegans* acts in germline and vulval development. *EMBO Rep.* 3:235–241.

Gonczy, P. 2002. Mechanisms of spindle positioning: focus on flies and worms. *Trends Cell Biol.* 12:332–339.

Gonczy, P., S. Pichler, M. Kirkham, and A.A. Hyman. 1999. Cytoplasmic dynein is required for distinct aspects of MTOC positioning, including centrosome separation, in the one cell stage *Caenorhabditis elegans* embryo. *J. Cell Biol.* 147:135–150.

Gueth-Hallonet, C., C. Antony, J. Aghion, A. Santa-Maria, I. Lajoie-Mazenc, M. Wright, and B. Maro. 1993. gamma-Tubulin is present in acentriolar MTOCs during early mouse development. *J. Cell Sci.* 105:157–166.

Gunning, B.E.S., and M.W. Steer. 1996. Coated vesicles. *In* Plant Cell Biology, Structure and Function. Jones and Bartlett Publishers, Sudbury, MA. 15.

Hamaguchi, Y. 2001. Displacement of the mitotic apparatus which induces ectopic polar body formation or parthenogenetic cleavage in starfish oocytes. *Dev. Biol.* 239:364–375.

Kamath, R.S., A.G. Fraser, Y. Dong, G. Poulin, R. Durbin, M. Gotta, A. Kanapin, N. Le Bot, S. Moreno, M. Sohrmann, et al. 2003. Systematic functional analysis of the *Caenorhabditis elegans* genome using RNAi. *Nature*. 421: 231–237.

Lawrence, C.J., R.K. Dawe, K.R. Christie, D.W. Cleveland, S.C. Dawson, S.A. Endow, L.S. Goldstein, H.V. Goodson, N. Hirokawa, J. Howard, R.L. Malmberg, J.R. McIntosh, H. Miki, T.J. Mitchison, Y. Okada, A.S. Reddy, W.M. Saxton, M. Schliwa, J.M. Scholey, R.D. Vale, C.E. Walczak, and L. Wordeman. 2004. A standardized kinesin nomenclature. *J. Cell Biol*. 2004. 167:19–22.

Li, S., C.M. Armstrong, N. Bertin, H. Ge, S. Milstein, M. Boxem, P.O. Vidalain, J.D.J. Han, A. Chesneau, T. Hao, et al. 2004. A map of the interactome network of the metazoan *C. elegans. Science.* 303:540–543.

Lutz, D.A., Y. Hamaguchi, and S. Inoue. 1988. Micromanipulation studies of the asymmetric positioning of the maturation spindle in *Chaetopterus sp*. oocytes: I. Anchorage of the spindle to the cortex and migration of a displaced spindle. *Cell Motil. Cytoskeleton.* 11:83–96.

Madl, J.E., and R.K. Herman. 1979. Polyploids and sex determination in *Caenorhabditis elegans. Genetics.* 93:393–402.

Mains, P.E., K.J. Kemphues, S.A. Sprunger, I.A. Sulston, and W.B. Wood. 1990. Mutations affecting meiotic and mitotic divisions of the early *Caenorhabditis elegans* embryo. *Genetics.* 126:593–605.

Maro, B., and M.H. Verlhac. 2002. Polar body formation: new rules for asymmetric divisions. *Nat. Cell Biol.* 4:E281–E283.

Maro, B., M.H. Johnson, S.J. Pickering, and G. Flach. 1984. Changes in actin distribution during fertilization of the mouse egg. *J. Embryol. Exp. Morphol.* 81:211–237.

Maro, B., M.H. Johnson, M. Webb, and G. Flach. 1986. Mechanism of polar body formation in the mouse oocyte: an interaction between chromosomes, the cytoskeleton and the plasma membrane. *J. Embryol. Exp. Morphol.* 92:11–32.

Navara, C.S., N.L. First, and G. Schatten. 1994. Microtubule organization in the cow during fertilization, polyspermy, parthenogenesis, and nuclear transfer: the role of the sperm aster. *Dev. Biol.* 162:29–40.

Palazzo, R.E., E. Vaisberg, R.W. Cole, and C.L. Rieder. 1992. Centriole duplication in lysates of *Spisula solidissima* oocytes. *Science.* 256:219–221.

Patel, N., D. Thierry-Mieg, and J.R. Mancillas. 1993. Cloning by insertional mutagenesis of a cDNA encoding *Caenorhabditis elegans* kinesin heavy chain. *Proc. Natl. Acad. Sci. USA.* 90:9181–9185.

Praitis, V., E. Casey, D. Collar, and J. Austin. 2001. Creation of low-copy integrated transgenic lines in *Caenorhabditis elegans. Genetics.* 157:1217–1226.

Sathananthan, A.H. 1997. Ultrastructure of the human egg. *Hum. Cell.* 10:21–38.

Saxton, W.M., M.E. Porter, S.A. Cohn, J.M. Scholey, E.C. Raff, and J.R. McIntosh. 1988. *Drosophila* kinesin: characterization of microtubule motility and ATPase. *Proc. Natl. Acad. Sci. USA.* 85:1109–1113.

Schuyler, S.C., and D. Pellman. 2001. Search, capture and signal: games microtubules and centrosomes play. *J. Cell Sci.* 114:247–255.

Selman, G.G. 1966. Cell cleavage in polar body formation. *Nature.* 210:750–751.

Sheeman, B., P. Carvalho, I. Sagot, J. Geiser, D. Kho, M.A. Hoyt, and D. Pellman. 2003. Determinants of *S. cerevisiae* dynein localization and activation: implications for the mechanism of spindle positioning. *Curr. Biol.* 13:364–372.

Signor, D., K.P. Wedaman, L.S. Rose, and J.M. Scholey. 1999. Two heteromeric kinesin complexes in chemosensory neurons and sensory cilia of *Caenorhabditis elegans. Mol. Biol. Cell.* 10:345–360.

Strome, S., J. Powers, M. Dunn, K. Reese, C.J. Malone, J. White, G. Seydoux, and W. Saxton. 2001. Spindle dynamics and the role of gamma-tubulin in early *Caenorhabditis elegans* embryos. *Mol. Biol. Cell.* 12:1751–1764.

Theurkauf, W.S., and R.S. Hawley. 1992. Meiotic spindle assembly in *Drosophila* females: behavior of nonexchange chromosomes and the effects of mutations in the nod kinesin-like protein. *J. Cell Biol.* 116:1167–1180.

Vale, R.D., T.S. Reese, and M.P. Sheetz. 1985. Identification of a novel force-generating protein, kinesin, involved in microtubule-based motility. *Cell.* 42:39–50.

Verlhac, M.H., C. Lefebvre, P. Guillaud, P. Rassinier, and B. Maro. 2000. Asymmetric division in mouse oocytes: with or without Mos. *Curr. Biol.* 10:1303–1306.

Wright, B.D., M. Terasaki, and J.M. Scholey. 1993. Roles of kinesin and kinesin-like proteins in sea urchin embryonic cell division: evaluation using antibody microinjection. *J. Cell Biol.* 123:681–689.

Yang, H.Y., K. McNally, and F.J. McNally. 2003. MEI-1/katanin is required for translocation of the meiosis I spindle to the oocyte cortex in *C. elegans. Dev. Biol.* 260:245–259.

Zhang, J., S. Li, R. Fischer, and X. Xiang. 2003. Accumulation of cytoplasmic dynein and dynactin at microtubule plus ends in *Aspergillus nidulans* is kinesin dependent. *Mol. Biol. Cell.* 14:1479–1488.

Zhang, Q.Y., M. Tamura, Y. Uetake, S. Washitani-Nemoto, and S. Nemoto. 2004. Regulation of the paternal inheritance of centrosomes in starfish zygotes. *Dev. Biol.* 266:190–200.